Biogeosciences Discuss., 10, 4575–4610, 2013
www.biogeosciences-discuss.net/10/4575/2013/
doi:10.5194/bgd-10-4575-2013
© Author(s) 2013. CC Attribution 3.0 License.

Biogeosciences Discussions
Open Access

This discussion paper is/has been under review for the journal Biogeosciences (BG).
Please refer to the corresponding final paper in BG if available.

Estimating temporal and spatial variation of ocean surface pCO_2 in the North Pacific using a Self Organizing Map neural network technique

S. Nakaoka[1], M. Telszewski[1,*], Y. Nojiri[1], S. Yasunaka[1], C. Miyazaki[1,], H. Mukai[1], and N. Usui[2]**

[1]National Institute for Environmental Studies, 16-2 Onogawa, Tsukuba, Ibaraki, 305-8506, Japan
[2]Meteorological Research Institute, 1-1 Nagamine, Tsukuba, Ibaraki, 305-0052, Japan
[*]now at: International Ocean Carbon Coordination Project, Institute of Oceanology of Polish Academy of Sciences, Ul. Powstańców Warszawy 55, 81-712 Sopot, Poland
[**]now at: Hokkaido University, Kita 8 Nishi 5, Kita-ku, Sapporo, Hokkaido, 060-0810, Japan

Received: 4 February 2013 – Accepted: 24 February 2013 – Published: 8 March 2013

Correspondence to: S. Nakaoka (nakaoka.shinichiro@nies.go.jp)

Published by Copernicus Publications on behalf of the European Geosciences Union.

Abstract

This study produced maps of the partial pressure of oceanic carbon dioxide (pCO_2^{sea}) in the North Pacific on a 0.25° latitude × 0.25° longitude grid from 2002 to 2008. The pCO_2^{sea} values were estimated by using a self-organizing map neural network technique to explain the non-linear relationships between observed pCO_2^{sea} data and four oceanic parameters: sea surface temperature (SST), mixed layer depth, chlorophyll *a* concentration, and sea surface salinity (SSS). The observed pCO_2^{sea} data was obtained from an extensive dataset generated by the volunteer observation ship program operated by the National Institute for Environmental Studies. The reconstructed pCO_2^{sea} values agreed rather well with the pCO_2^{sea} measurements, the root mean square error being 17.6 µatm. The pCO_2^{sea} estimates were improved by including SSS as one of the training parameters and by taking into account secular increases of pCO_2^{sea} that have tracked increases in atmospheric CO_2. Estimated pCO_2^{sea} values accurately reproduced pCO_2^{sea} data at several stations in the North Pacific. The distributions of pCO_2^{sea} revealed by seven-year averaged monthly pCO_2^{sea} maps were similar to Lamont-Doherty Earth Observatory pCO_2^{sea} climatology and more precisely reflected oceanic conditions. The distributions of pCO_2^{sea} anomalies over the North Pacific during the winter clearly showed regional contrasts between El Niño and La Niña years related to changes of SST and vertical mixing.

1 Introduction

The ocean plays an important role as a major carbon reservoir for CO_2 emitted to the atmosphere from fossil fuel burning, cement production, and biomass burning. The ocean has absorbed about 48 % of the CO_2 emitted to the atmosphere by fossil-fuel combustion since the Industrial Revolution (Sabine et al., 2004). To evaluate the global budget of oceanic CO_2 uptake, measurements of the partial pressure of CO_2 (pCO_2^{sea}) in surface seawater have been carried out over the global ocean, with the highest

BGD
10, 4575–4610, 2013

intensity in the equatorial Pacific (Feely et al., 1987, 2006; Ishii et al., 2009), the North Atlantic (Cooper et al., 1998; Olsen et al., 2003; Schuster et al., 2009), and the North Pacific (Inoue et al., 1995; Murphy et al., 2001a; Zeng et al., 2002; Chierici et al., 2006). A compilation of worldwide efforts to measure pCO_2^{sea} on a global scale can be found in Takahashi et al. (2009). The authors led by a team at the Lamont-Doherty Earth Observatory (LDEO) computed a 35-yr pCO_2^{sea} climatology (for a reference year 2000) on 4° latitude × 5° longitude resolution and estimated the annual global air-sea CO_2 exchange at -1.6 ± 0.9 PgC yr^{-1}.

Neural network (NN) techniques can be generally described as empirical statistical tools that resolve, to certain degree, the non-linear, often discontinuous relationships among proxy parameters without any a priori assumptions. In the past decade a handful of authors reported the application of an NN technique to basin-scale pCO_2^{sea} analysis (e.g. Lefèvre et al., 2005; Jamet et al., 2007; Friedrich and Oschlies, 2009a,b; Telszewski et al., 2009) concentrating mainly on the North Atlantic Ocean. Most recently, Telszewski et al. (2009) successfully applied a Self Organizing Map (SOM) based NN technique to reconstruct pCO_2^{sea} distribution in the North Atlantic (10.5° N to 75.5° N, 9.5° E to 75.5° W) for three years (2004–2006) by examining non-linear/discontinuous relationship between pCO_2^{sea} and ocean parameters of sea surface temperature (SST), mixed layer depth (MLD) and chlorophyll *a* concentration (CHL). One of the main benefits of this approach over the more traditional techniques such as the multiple linear regression is that there are numerous empirical relationships established (e.g. 2220 in Telszewski et al., 2009) between examined parameters allowing for more accurate representation of the highly variable system of interconnected water properties.

The North Pacific is dominated by two major current systems: the subarctic and subtropical gyres (Fig. 1). The cold Oyashio Current and the warm Kuroshio Current are the western boundary currents of the North Pacific subarctic and subtropical gyres, respectively. The two currents meet at mid-latitudes in the western North Pacific and turn toward the east as the North Pacific Current. The North Pacific has been typically characterized as a high-nutrient, low-chlorophyll region of the ocean at high latitudes

BGD
10, 4575–4610, 2013

because of the low influx of iron to the ocean surface (Dugdale and Wilkerson, 1991) and as a low-nutrient, low-chlorophyll region at low latitudes (Karl and Letelier, 2008). The subarctic North Pacific is an upwelling area, within which the transport of nutrient- and CO_2-rich subsurface water to the surface assures high biological productivity in spring and summer. In the North Pacific there are thus quite large temporal and spatial variations of pCO_2^{sea}, the regional characteristics of which are generally understood from the LDEO climatology (Takahashi et al., 2009).

For analysis of temporal variability of pCO_2^{sea} in the North Pacific, Takamura et al. (2010) used multiple linear regression (MLR) analysis to reconstruct pCO_2^{sea} distributions as a function of SST and sea surface salinity (SSS) from 1999 to 2006 in mid-latitudes (25° N to 40° N, 120° W to 150° W, 140° E to 170° E). They resolved regional differences in secular increasing trends of pCO_2^{sea}, however their MLR technique could not be applied to spatial mapping. Sarma et al. (2006) used MLR relationships to estimate pCO_2^{sea} from SST and satellite-based CHL observations in highlatitude regions of the eastern and western North Pacific, but the applicability of the MLR equations was limited to spring and summer.

The precise timeseries analyses of pelagic ocean pCO_2^{sea} variability are limited to timeseries stations (Bates, 2007; Dore et al., 2009) where monthly pCO_2^{sea} observations are available over extended time periods. Two areas of frequent shipboard observations of pCO_2^{sea} other than timeseries stations are the eastern and western equatorial Pacific (Feely et al., 2006; Ishii et al., 2009), where apparent interannual pCO_2^{sea} variations are known to occur as a result of the El Niño-Southern Oscillation (ENSO). Another place where there have been frequent shipboard pCO_2^{sea} observations in the North Pacific is the 137° E repeat line (Midorikawa et al., 2006), where a weak but significant relationship between pCO_2^{sea} and ENSO has been observed. A basin-wide analysis of observed pCO_2^{sea} variability (including the analysis of the interannual signal) has not yet been successfully performed. An atmospheric CO_2 inverse model (Patra et al., 2005) and an ocean biogeochemical model (Valsala et al., 2012), however, suggest the possible correlation of the pCO_2^{sea} variability with Pacific Decadal Oscillation (PDO).

BGD
10, 4575–4610, 2013

Our goal in this study was to reconstruct temporal and spatial variability of the pCO_2^{sea} distribution in the North Pacific for seven years from 2002 to 2008 using the SOM technique applied to observational pCO_2^{sea} dataset obtained by the NIES VOS program. We then compared the estimated pCO_2^{sea} values with measured pCO_2^{sea} values obtained from the NIES VOS program and other datasets in various areas of the North Pacific (Fig. 1). We also presented the change of the pCO_2^{sea} distribution in response to the ENSO events.

2 Method and datasets

2.1 Method of pCO_2^{sea} estimation

The study area includes the North Pacific from 10° N to 60° N and from 120° E to 90° W and is hereafter called the North Pacific, although we excluded coastal (bathymetric depth < 500 m) and ice-covered (SST < −1.8 °C) areas from the analysis. In this study, we hypothesized that pCO_2^{sea} could be estimated by a linear function of time and an SOM function (f_{SOM}) of four independent variables: SST, MLD, CHL, and SSS. The equation for pCO_2^{sea} then takes the following form:

$$pCO_2^{sea} = a^*(t - t_{ref}) + f_{SOM}(SST, MLD, CHL, SSS) \quad (1)$$

In Eq. (1) "a" is the secular rate of change of atmospheric CO_2 in µatm day^{-1}, "t" denotes the date, and the reference date "t_{ref}" is set to 30 June 2005. The use of SSS in this study is consistent with the suggestion by Telszewski et al. (2009). In addition, we assumed pCO_2^{sea} to be a linear function of time to take into account the influence of anthropogenic CO_2 emissions on pCO_2^{sea}, an effect that could not be accounted for by SST, MLD, CHL, or SSS. The anthropogenic influence on pCO_2^{sea} is considered negligeble for relatively short analyses e.g. three years (cf., Lefèvre et al., 2005; Telszewski et al., 2009), but it builds up to around 10 µatm after seven years. Midorikawa et al. (2006) reported that the secular trend of pCO_2^{sea} varied from 1.3 to 1.8 µatm yr^{-1}

BGD
10, 4575–4610, 2013

(close to the rate of increase of atmospheric CO_2) in the western subtropical North Pacific based on their measurements over 20 yr along 137° E. Wong et al. (2010) also reported that their 30-yr time series of measurements along line P showed that the long-term trend of pCO_2^{sea} tracked the increase of atmospheric CO_2 in the eastern subarctic region. Takahashi et al. (2006) concluded that for the most part the increase of oceanic CO_2 in the North Pacific followed the increase of atmospheric CO_2 for the last 35 yr. We assumed in this study that the secular trend of pCO_2^{sea} was approximately a constant fraction of the rate of change of atmospheric CO_2 over the North Pacific. Specifically, we assumed the value of the coefficient a in Eq. (1) to be 4.82×10^{-3} (= 1.76/365.285) µatm day^{-1}, which is the rate of increase of atmospheric CO_2 concentration converted from the CO_2 mole fractions (xCO_2^{air}) in the GlobalVIEW-CO_2 dataset (GLOBALVIEW-CO2, 2011) for the North Pacific region during the period of analysis.

The method for reconstructing pCO_2^{sea} is based on the methodology of Telszewski et al. (2009), but we allocated about three times as many neurons on a flat sheet map (53 × 115) to improve the estimate. A neuron in this study is a vector that has four components: SST, MLD, CHL, and SSS. The values of these components, the training dataset, are prospectively normalized linearly (SST, SSS) or logarithmically (MLD, CHL) to create an even distribution among the input variables (cf., Fig. 3 of Telszewski et al., 2009). As indicated schematically in Fig. 2, three processes are executed in order to estimate basin-wide pCO_2^{sea} fields in the SOM analysis procedure.

First, a neuron's weight vectors ($\boldsymbol{x}_i$), which are linearly initialized, are repeatedly trained by input vectors ($\boldsymbol{y}_j$), by being presented with the normalized SST, MLD, CHL, and SSS values, until the statistical composition of the training dataset is extracted and the neural network sufficiently represents the non-linear inter-dependence of proxy parameters used in training (Training Process in Fig. 2a). At each step, Euclidean distances (D) are calculated between the weight vectors of neurons and the input vector:

$$D(\boldsymbol{x}_i, \boldsymbol{y}_j) = \left[(x_{i\_SST} - y_{j\_SST})^2 + (x_{i\_MLD} - y_{j\_MLD})^2 + (x_{i\_CHL} - y_{j\_CHL})^2 + (x_{i\_SSS} - y_{j\_SSS})^2\right]^{0.5} \quad (2)$$

BGD
10, 4575–4610, 2013

The neuron closest to the training data point in Euclidean distance terms, here called the winner, is adjusted towards its value by a fraction of this distance dictated by the linearly time-decreasing learning function. At the same time, the neurons in the vicinity of the winner are also adjusted towards the value of the training data point, by a fraction of winner's adjustment in accordance with time-decreasing Gaussian function, as explained by Kohonen (2001). This process results in clustering of similar neurons and self-organization of the map. The observed pCO_2^{sea} dataset is not required at this stage of the analysis.

Second, each neuron is labeled with an observed pCO_2^{sea} value. Technically, the labeling process follows the same principles as the training process. The labeling data, which in this study consists of the observed pCO_2^{sea} value assigned to a reference year by adding/subtracting the assumed temporal change of pCO_2^{sea} and coincided with normalized SST, MLD, CHL, and SSS values, is presented to the neural network and a winner neuron is found (Labeling Process in Fig. 2b). Instead of adjusting the winner's value, it is labeled with the pCO_2^{sea} value of the labeling data. This process is carried out for each of the observed pCO_2^{sea} values. After the labeling process, most neurons are labeled with a pCO_2^{sea} value. Neurons are consequently represented by five-dimensional vectors.

Third, the labeled SOM neurons are used to assign pCO_2^{sea} values to the geographical grid points of the North Pacific (Mapping Process in Fig. 2c). The initial training data set is being presented to the trained and labeled SOM map. Upon computing the winner neuron, no adjustments are being made. Instead, the training data is assigned a pCO_2^{sea} value of the winner neuron. This value becomes a pCO_2^{sea} estimate for time and location determined by the spatio/temporal coordinates of each training data.

The reconstructed pCO_2^{sea} distributions obtained as a result of this work will be available for scientific purposes at the website http://soop.jp.

BGD
10, 4575–4610, 2013

2.2 Training data set (SST, MLD, CHL, SSS)

We used four high-resolution datasets, one for SST, MLD, CHL, and SSS to train the SOM. We obtained observed SST datasets from the Merged satellite and in situ data Global Daily Sea Surface Temperatures (MGDSST) Project (http://goos.kishou.go.jp/rrtdb/database.html) at a daily frequency and 0.25° latitude × 0.25° longitude resolution (Kurihara et al., 2006). We obtained daily assimilated MLD estimates from the GLobal Ocean ReanalYses and Simulations (GLORYS) model by Mercator Ocean (Le Centre National de la Recherche Scientifique, France) with a horizontal resolution of 0.25° latitude × 0.25° longitude (Bernard et al., 2006; Ferry et al., 2010). Satellite CHL data were obtained from MODIS-Aqua and SeaWiFS Level 3 Standard products provided by NASA/GFSC/DAAC at a frequency of eight per day and resolution of 9 km (http://oceancolor.gsfc.nasa.gov). We obtained assimilated SSS estimates from the MOVE/MRI.COM-NP model of the Meteorological Research Institute, Japan at a frequency of 10 per day and horizontal resolution of 0.5° latitude and 0.5° longitude (Usui et al., 2006). For the analysis all parameters were re-gridded onto a frequency of one per day and horizontal resolution of 0.25° latitude × 0.25° longitude.

2.3 pCO_2^{sea} datasets for labeling

To estimate pCO_2^{sea} fields in the North Pacific, it was necessary to label the trained SOM neurons with pCO_2^{sea} values. In the labeling process, observed pCO_2^{sea} data together with corresponding SST, MLD, CHL and SSS values were needed. We used a subset of the North Pacific dataset collected by the NIES VOS program. The pCO_2^{sea} data is available for public use on the web page http://soop.jp. Information related to the four VOS lines is summarized in Table 1, and their composite cruise routes are depicted in Fig. 3. The commercial ships collaborating in the NIES-VOS program have taken part in trans-Pacific cruises between Japan and North America (10° N to 55° N, 140° E to 230° E) since March 1995 and between Japan and Oceania (45° S to 35° N, 140° E to 180° E) since July 2006. The ships have sailed regularly at intervals of about

BGD
10, 4575–4610, 2013

5–8 weeks between Japan and North America or Oceania. The volunteer ship that has sailed to North America sailed to the northern part of North America in the early part of the NIES-VOS program but since 2003 the route has occasionally shifted to the southeast to pass through the Panama Canal (Supplement Fig. 1). In contrast, the ship that has sailed between Japan and Oceania has sailed regularly as a member of a bi-weekly service fleet and the shipping route has been mostly fixed.

Although we reconstructed pCO_2^{sea} in the North Pacific after 2002, in the analysis we used some in situ data for years 1998–2001 due to the insufficient data coverage especially in the subarctic region for years 2002–2008. The addition of pCO_2^{sea} data from 1998 to 2001 to the labeling dataset improved the coverage of monthly measurements (Supplement Fig. 2). The improved coverage facilitated reproduction of the rapid drawdown of pCO_2^{sea} due to phytoplankton photosynthesis during the spring bloom in the highly productive western mid-high latitude region.

Murphy et al. (2001b) and Fransson et al. (2006) have described the ocean surface CO_2 measurement system used by the NIES VOS program. The non-dispersive infrared analyzer used for those measurements was changed from a Licor 6262 to a Licor 7000 for the M/S *Pyxis* cruises in 2006 (Table 1). The CO_2 standard gases were calibrated by the NIES and are traceable to the World Meteorological Organization scale. The flow-through tandem equilibrator provides a continuous pCO_2^{sea} output with high temporal resolution (Murphy et al., 2001b). The pCO_2^{sea} measurements were made every 10 s and the pCO_2^{sea} data were 10 min averages of those measurements accompanied by supplementary values of observed atmospheric and oceanic parameters. The pCO_2^{sea} data were then averaged on a daily basis within 0.25° latitude × 0.25° longitude grid boxes. Consequently, the number of pCO_2^{sea} data by the NIES VOS program amounted to 317 332 and a total of 73 284 pCO_2^{sea} data were binned as the labeling dataset.

BGD
10, 4575–4610, 2013

2.4 Other oceanic CO_2 datasets used for the validation of estimated pCO_2^{sea}

To validate pCO_2^{sea} values reconstructed by the SOM analysis, we used the fugacity of oceanic CO_2 (fCO_2^{sea}) dataset from the Surface Ocean CO_2 ATlas (SOCAT; http://www.socat.info) database. That dataset has been in the public domain since September 2011 and has been subject to quality control as a part of an international collaboration of more than 10 institutes (including the NIES) which work on ocean surface CO_2 observations (Pfeil et al., 2012). In the North Pacific, the SOCAT database contains the fCO_2^{sea} values measured mainly by NIES, the Japan Meteorological Agency (JMA), the Japan Agency for Marine-Earth Science and Technology (JAMSTEC), and the United States National Oceanic and Atmospheric Administration (NOAA). The average bias between the observed pCO_2^{sea} and fCO_2^{sea} values was calculated to be 0.3 ± 0.1 %. No corrections were made when comparing the two datasets because the uncertainty of the estimated pCO_2^{sea} values was much larger than the difference (see Sect. 2.7.1 for details).

Underway pCO_2^{sea} data and mooring pCO_2^{sea} data collected by Wong and Johannessen (2010) and Sabine et al. (2010), respectively, were obtained from the Carbon Dioxide Information Analysis Center (CDIAC; http://cdiac.ornl.gov/oceans/). We used those data for the comparisons near Ocean Station P (50° N, 145° W). In addition, we used pCO_2^{sea} values calculated from measurements of dissolved inorganic carbon (DIC) and total alkalinity (TA) at two stations: Station KNOT (44° N, 155° E; Wakita et al., 2010) and Station ALOHA (23° N, 158° W; Dore et al., 2009).

2.5 Ranges of the training/labeling dataset

As explained by Telszewski et al. (2009), one of the biggest advantages of SOM analysis over the more traditional methods is the fact that the temporal and spatial distribution of proxy parameters in the training and labeling datasets does not influence the analysis. Instead ranges covered by these parameters in each dataset, and more precisely their relative overlap determines whether the SOM will be able to reconstruct the

BGD
10, 4575–4610, 2013

distribution of the predicted parameter. Ranges of the training/labeling datasets and the trained neurons are summarized in Table 2. The training dataset SSTs varied between −1.8 °C and 32.7 °C; the MLD ranged from 1 m to more than 500 m; CHL varied from 0 to more than 10 mg m^{-3}; and the range of SSS was 30.15–35.69. The values in the labeling datasets and neurons covered most of the range of values in the training dataset. However, the maximum MLDs in the labeling dataset (416 m) and in the neurons (194 m) were substantially lower than the maximum MLD in the training dataset (> 500 m; Table 2). Our results indicate that the correlation between pCO_2^{sea} and MLD was not apparent when the MLD was deeper than 200 m (not shown), a result also reported for the North Atlantic by Telszewski et al. (2009).

2.6 Reconstructing pCO_2^{sea} distributions in winter at high latitudes

The three products, SST, MLD, and SSS, provided full basin-wide coverage from 2002 to 2008. However, the CHL data were affected by the lack of satellite coverage from November to January at high latitudes of the North Pacific (north of 45° N) due to the low-angle of the sun during that time and enormous atmospheric correction required to retrieve the signal. To reconstruct pCO_2^{sea} for this area during those months, we assumed that pCO_2^{sea} could be adequately characterized by only three parameters: SST, MLD and SSS. The rationale for this assumption is that biological activity is relatively low during the winter at high latitudes (e.g. Imai et al., 2002). Therefore, we prepared another SOM trained by three parameters SST, MLD and SSS. We generated complete pCO_2^{sea} maps in the study area by combining the pCO_2^{sea} values obtained with the fourparameter SOM including CHL with the values obtained with the three-parameter SOM excluding CHL in the area north of 45° N during the period from November to January. We checked the difference between the pCO_2^{sea} values estimated with the four-parameter SOM and the three-parameter SOM in the region between 40° N and 45° N and found the difference to be negligibly small from November to January because of the relatively low biological activity during that time. The implication is that combining the results from the two SOMs does not produce any bias.

BGD
10, 4575–4610, 2013

2.7 Uncertainty and improvement of the pCO_2^{sea} estimate

2.7.1 Uncertainty

For each in situ pCO_2^{sea} measurement, the corresponding SOM pCO_2^{sea} estimate was determined on the basis of the spatial (0.25° longitude × 0.25° latitude grid) and temporal (daily intervals between 1 January 2002 and 31 December 2008) coordinates associated with the measurement. We calculated the root mean square error (RMSE) between observed pCO_2^{sea} and estimated pCO_2^{sea} values as follows:

$$\mathrm{RMSE} = \sqrt{\frac{\sum \left(pCO_2^{sea}(\mathrm{estimated})^2 - pCO_2^{sea}(\mathrm{observed})^2\right)}{n}} \quad (3)$$

where n is the number of points in the labeling dataset. The RMSE provided an estimate of the uncertainty of the method in reproducing the in situ measurements and equaled 17.6 µatm, or 5.0 % of the average pCO_2^{sea} of the in situ dataset. A scatter plot of the estimated pCO_2^{sea} against the observed pCO_2^{sea} (Fig. 4) shows that the values are clustered around the 1 : 1 line with slightly more scatter at high pCO_2^{sea} over 400 µatm.

Zeng et al. (2002) estimated the distribution of monthly average pCO_2^{sea} in the North Pacific based on data from the NIES VOS program from 1995 to 1999 and reported that the estimated pCO_2^{sea} agreed with the in situ pCO_2^{sea} to within a RMSE of 24.9 µatm. Sarma et al. (2006) used a MLR method to estimate the distribution of monthly average pCO_2^{sea} in the North Pacific during the spring-summer period in 1998 and reported that the derived pCO_2^{sea} agreed with the shipboard pCO_2^{sea} observations to within a RMSE of 17–23 µatm. Although the present study represents a much longer period of time than the previous reports, the RMSE achieved in this study is comparable to or better than the RMSEs achieved in the shorter studies.

BGD
10, 4575–4610, 2013

2.7.2 Improvement in the NN scheme

We have implemented two major improvements over the previous attempt to utilize SOM neural network to compute the pCO_2^{sea} distribution. In the first one we followed the suggestion of Telszewski et al. (2009) to use the SSS dataset as one of the training datasets to improve pCO_2^{sea} estimates. To quantify the improvement achieved by using the SSS dataset, we generated another pCO_2^{sea} map derived with a three-parameter SOM that excluded SSS and compared the result with the four-parameter SOM result. The RMSE of the three-parameter SOM estimate was 20.0 µatm. Use of SSS in the training dataset therefore reduced the RMSE by 12 %. The pCO_2^{sea} distributions were also improved by the use of the SSS data. To visualize the differences, we mapped seven-year averaged monthly pCO_2^{sea} distributions in February and August derived with and without inclusion of SSS in the training dataset (Fig. 5). The estimated pCO_2^{sea} derived from the three-parameter SOM in February is characterized by a smaller longitudinal difference in mid latitudes than the pCO_2^{sea} derived from the four-parameter SOM. Furthermore, use of the four-parameter SOM enabled reconstruction of quite high pCO_2^{sea} values in August in the eastern low/mid-latitude region, where the North Pacific current flows, whereas use of the three-parameter SOM failed to reproduce this feature. Figure 6 shows the temporal variation of pCO_2^{sea} derived with the two SOMs in the region (37° N, 140° W). It clearly shows that the agreement between observed and estimated pCO_2^{sea} values was better for the four-parameter SOM than the three-parameter SOM. The RMSE in the region was improved from 15.9 µatm to 10.6 µatm by inclusion of SSS. The improvement was especially apparent during the summer when high pCO_2^{sea} values (about 400 µatm) were observed. The reason why inclusion of SSS improved the pCO_2^{sea} estimate is unclear. Inclusion of SSS in the SOM analysis may facilitate differentiation between temporal and spatial oceanic variability that could not be elucidated with only SST, MLD, and CHL.

Taking into account the influence of anthropogenic CO_2 emissions on the trend of pCO_2^{sea} was the second improvement introduced by this work. As described above it

BGD
10, 4575–4610, 2013

was done by adding or subtracting 1.76 µatm yr^{-1} (4.82×10^{-3} µatm day^{-1}) to project observed pCO_2^{sea} values to the pCO_2^{sea} values in the reference year of 2005 (Eq. 1). The improvement of the pCO_2^{sea} estimate by making this correction was not spatially uniform. For example, the RMSEs were reduced by adding the term from 10.2 µatm to 9.1 µatm in the Station P area, from 8.8 µatm to 7.4 µatm in the WST area, and from 10.8 µatm to 7.9 µatm in the Station ALOHA area. In contrast, the improvements at Station KNOT area and the KE area were unclear (see in Fig. 1). Overall, inclusion of the secular trend effect slightly, but statistically significantly ($p < 0.05$), reduced the RMSE for the whole of the North Pacific.

3 Temporal and spatial variation of pCO_2^{sea}

3.1 Mapping of seven-year averaged monthly pCO_2^{sea} distributions

Figure 7 presents a comparison of seven-year (2002 to 2008) averaged monthly pCO_2^{sea} distributions derived from SOM results for February, May, August, and November with LDEO pCO_2^{sea} climatology (Takahashi et al., 2009). The comparison reveals that the reconstructed pCO_2^{sea} maps are generally similar to the LDEO climatology however the resolution of the SOM estimated pCO_2^{sea} distributions is much higher, and the results more precisely resolve some oceanic features. Both studies show high pCO_2^{sea} values (over 400 µatm) at high latitudes in the North Pacific in February, however the SOM reconstructed pCO_2^{sea} distribution shows pCO_2^{sea} rich water between the Bering Sea and the coast of northern Japan along the axis of the cold, southward-flowing Eastern Kamchatka Current. As described in Sect. 2.7.2, high pCO_2^{sea} values are apparent from June to October in the eastern low/mid-latitude region, where the North Pacific Current and the California Current flow, and the high pCO_2^{sea} field dominates. With respect to the coastal region, low estimates of pCO_2^{sea} stretch along the coastline from the Aleutian Islands to the California Peninsula from May to October, when the concentration of phytoplankton is high.

BGD
10, 4575–4610, 2013

The reconstructed pCO_2^{sea} distributions in this study clearly show a tongue of very low pCO_2^{sea} (about 320 µatm) water distributed (except in August) uniformly between the western and central mid-latitude regions of the North Pacific (Fig. 7). Such low pCO_2^{sea} values are attributed to high rates of photosynthesis (Kameda, 2003) and cooling of the seawater that occurred mainly in the subtropics. In addition, a band of relatively high pCO_2^{sea} caused mainly by a seasonal rise in temperature was also apparent during the period from May to September in the western North Pacific between 15° N and 30° N. The temperature rise began in April and amounted to about 2–5 °C. Following the temperature dependence of pCO_2^{sea} given by Takahashi et al. (1993), $\delta \ln pCO_2^{sea} / \delta T = 0.0423\,^{\circ}C^{-1}$, the expected pCO_2^{sea} rise due to the temperature effect is about 30–70 µatm. The observed increase in expected pCO_2^{sea} is only about half of the expected pCO_2^{sea} rise due to temperature effects. The increase may have been attenuated by other factors such as photosynthetic uptake of CO_2.

3.2 Reproducibility of temporal pCO_2^{sea} variations in each of six regions

To facilitate a discussion about the temporal variations of pCO_2^{sea} in the North Pacific, Fig. 8 shows the time series of area-averaged pCO_2^{sea} estimated in this study along with the estimates of Takamura et al. (2010). The grid size of all the averaged areas except in the Station KNOT area is set to 4° latitude × 5° longitude, whereas the Station KNOT area is set to 43.5° N to 45.5° N, 153° E to 157° E to exclude the transition zone between the Kuroshio and the Oyashio. The panels in Fig. 8 also include comparisons between the observed pCO_2^{sea} data from various observation programs and the data from the NIES VOS program in the same area. The estimated pCO_2^{sea} values at each location generally agree well with observed values and other estimates, most of the data lying within the spatial variability (twice the spatial standard deviation; 2-σ) calculated for each area. However disagreements greater than 20 µatm between estimated pCO_2^{sea} and observed pCO_2^{sea}, as exemplified in the area surrounding Station KNOT (Fig. 8a), occur occasionally. The calculated pCO_2^{sea} in Station P area generally agree well with

BGD
10, 4575–4610, 2013

the data from the NIES VOS program as well as with pCO_2^{sea} values measured by an underway system from 2002 to 2003 and by a moored buoy system from 2007 to 2008 (Fig. 8b). The largest seasonal amplitudes tend to coincide with the largest disagreements between the estimates (Zeng et al., 2002). The calculated pCO_2^{sea} values in the KE area of the eastern mid-latitude region (Fig. 8c) agree well with the NIES dataset as well as with the fCO_2^{sea} values from the SOCAT dataset, all pCO_2^{sea} values lying within the spatial variability. The results of Takamura et al. (2010) also agree with the pCO_2^{sea} measurements to within 15–20 µatm, and the temporal pattern of those data is generally consistent with the pCO_2^{sea} estimates within the spatial variability from this study. The temporal variations of pCO_2^{sea} in the WST area (Fig. 8d) and Station ALOHA area (Fig. 8e) agree well with the pCO_2^{sea} values in the SOCAT dataset, even though the observed pCO_2^{sea} data used for the labeling process in the SOM analysis rarely existed in these areas. The calculated pCO_2^{sea} values in the EST area (Fig. 8f) also agree well with the data from the NIES VOS program. As shown in the Fig. 8d–f, the patterns of variation were similar in the WST area, the Station ALOHA area, and the EST area. Keeping in mind that only data obtained by the NIES VOS program were used in the SOM labeling process, these results suggest that the labeling process allows labeled SOM neurons to effectively learn pCO_2^{sea} variations from pCO_2^{sea} values observed in other subtropical areas. This confirms the notion that the SOM technique overcomes problems associated with temporal and spatial data scarcity.

3.3 Difference of pCO_2^{sea} distributions during ENSO events

The ENSO has a large influence on the climate of the North Pacific (IPCC, 2007), and large fluctuations of pCO_2^{sea} coincided with the ENSO cycle have also been observed in the equatorial Pacific (Feely et al., 2006; Ishii et al., 2009). Based on their measurements from 1983 to 2003, Midorikawa et al. (2006) have suggested that the interannual variation of pCO_2^{sea} in the western subtropical North Pacific is also related to the ENSO. Although the extent of the ENSO influence on oceanic and atmospheric variables is known to be global (Trenberth and Caron, 2000), the impact of the ENSO

BGD
10, 4575–4610, 2013

on the distribution of pCO_2^{sea} over the entire area of the North Pacific is not well understood. Figure 9 depicts the estimated distributions of the de-trended pCO_2^{sea}, SST, and MLD anomalies during the winters of 2003 (i.e. El Niño) and 2008 (i.e. La Niña). Anomalies in Fig. 9 are deviations from the monthly climatology for the period of 2002–2008. El Niño/La Niña periods were chosen in accordance with JMA's definition based on the five-month running mean SST deviation for the NINO.3 region (5° S to 5° N, 150° E to 90° E).

The patterns of SST anomalies in Fig. 9 are typical of El Niño and La Niña winters (Trenberth and Caron, 2000). The pCO_2^{sea} anomaly related to ENSO events is easily discernible in the western-central subtropical region, in the eastern subarctic region, and in the eastern mid-latitude region south of 30° N. For example, a negative pCO_2^{sea} anomaly is apparent in the western-central subtropical region in 2003 (El Niño), when the SST anomaly was negative; whereas a positive pCO_2^{sea} anomaly is apparent in 2008 (La Niña), when the SST anomaly is positive. The opposite pattern is observed for the eastern mid-latitude region south of 30° N. The amplitudes of the associated pCO_2^{sea} anomalies are about 15 µatm, and their SST amplitudes are 1 °C. The pCO_2^{sea} change closely tracked the SST change in accordance with the iso-chemical temperature dependency of Takahashi et al. (1993).

A negative relationship between pCO_2^{sea} and SST is apparent in the eastern subarctic North Pacific, where the signal of thermodynamic changes on variations of pCO_2^{sea} was opposite to that seen in the subtropics. As indicated in Fig. 9, the MLD anomaly clearly showed the pattern typical of ENSO events (Alexander et al., 2002). In contrast, the MLD was deeper in 2008 than in 2003 in the eastern subarctic region. This result indicates that more CO_2-rich subsurface water was entrained into surface waters during the La Niña period than during the El Niño period.

BGD
10, 4575–4610, 2013

4 Summary

In this study we used the SOM technique of Telszewski et al. (2009) to examine the temporal and spatial variations of pCO_2^{sea} in the North Pacific during the period 2002–2008. To improve the pCO_2^{sea} estimates, we used SSS as an additional training parameter and assumed a trend of increasing pCO_2^{sea} to take into account the effect of anthropogenic CO_2 emissions on pCO_2^{sea}. The estimated results revealed that the SOM technique could satisfactory reconstruct variations of pCO_2^{sea} associated with bio-geophysical processes expressed by the variability in four proxy parameters: SST, MLD, CHL and SSS. We calculated the uncertainty of the pCO_2^{sea} estimation to be 17.6 µatm. The fact that the uncertainty was reduced by about 12 % by inclusion of SSS in the training dataset suggests that SSS can be a useful parameter for the estimation of temporal and spatial variation of pCO_2^{sea}. We also found that pCO_2^{sea} estimates were improved by taking account of the temporal trend associated with anthropogenic CO_2 emissions.

The calculated pCO_2^{sea} variations in six ocean areas generally agreed well not only with the NIES VOS program pCO_2^{sea} data used for the labeling process but also with other in situ pCO_2^{sea} datasets. Seven-year (2002–2008) averaged monthly pCO_2^{sea} distributions were similar to 35-yr climatology pCO_2^{sea} distributions (Takahashi et al., 2009). However, the SOM-based pCO_2^{sea} mapping with its high spatial resolution reflected oceanic conditions with more accuracy. The estimated inter-annual pCO_2^{sea} variability revealed a difference in the spatial pattern of pCO_2^{sea} during the winter of the El Niño period in 2003 and the La Niña period in 2008. A negative pCO_2^{sea} anomaly was apparent in 2003 in the western subtropical North Pacific and in the eastern subarctic North Pacific off the coast of Alaska, whereas a positive anomaly was apparent in 2008 in the same regions. In the western subtropical and eastern mid-latitude regions, the correlation of the pCO_2^{sea} variability with ENSO events seemed to be related mainly to changes in the thermodynamic properties of seawater. In contrast, similar correlation

BGD
10, 4575–4610, 2013

in the subarctic North Pacific seemed to be related to changes in vertical transport of CO_2 rich subsurface waters.

Further improvement of pCO_2^{sea} estimates will require an increase in the number of data points used for labeling to reduce the pCO_2^{sea} error. We plan to undertake a longer-term study using the community quality controlled (Pfeil et al., 2012) SOCAT collection as the labeling dataset. The number of neurons is also crucial for accurate pCO_2^{sea} estimation. In this study we used three times as many neurons as Telszewski et al. (2009) to achieve adequate reproducibility of the pCO_2^{sea} estimates. However, the number of neurons used in this study was determined not by scientific analysis, but was based on the available computing power. More sensitivity studies are needed to determine the relationship between the estimated error and the number of neurons. It might also be possible to improve the pCO_2^{sea} estimate by inclusion of more ocean parameters. Sea surface height is a potential training parameter with basin-wide coverage. Even if sea surface height cannot be directly related to pCO_2^{sea} variations, a combination of parameters can be used to identify location and time more precisely.

In addition to estimates in the North Pacific, long-term global pCO_2^{sea} mapping based on such measurements is also important for understanding inter-annual variations of air-sea CO_2 exchanges. Although pCO_2^{sea} variations related to climate changes such as the PDO have been reported (Valsala et al., 2012), the overall impact of such changes on global pCO_2^{sea} variations is not well understood. In the present study, the study area was confined to the North Pacific. However, the SOM technique used in the present study has the potential to estimate pCO_2^{sea} in regions where there are insufficient numbers of observations, and such regions will be our next target. It is axiomatic to say that further pCO_2^{sea} measurements are critical, especially in the South Pacific, where few pCO_2^{sea} measurements have been made (Sabine et al., 2012).

Supplementary material related to this article is available online at: http://www.biogeosciences-discuss.net/10/4575/2013/bgd-10-4575-2013-supplement.pdf.

BGD
10, 4575–4610, 2013

Acknowledgements. We deeply appreciate Seaboard International Shipping Co., Mitsui O. S. K. Lines Co, Toyofuji Shipping Co. and Kagoshima Senpaku Co. for their generous cooperation with the NIES VOS program. We would like to thank the crew of the M/S *Skaugran*, M/S *Alligator Hope*, M/S *Pyxis*, and M/S *Trans Future 5*. We also thank S. Kariya and T. Yamada of the Global Environmental Forum for their constant assistance with the observations and appreciate K. Katsumata for calibrating the CO_2 standard gases. We gratefully acknowledge the Mercator Ocean for providing the GLORYS model output. The research was financially supported by the Global Environment Research Account for National Institutes by the Ministry of Environment, Japan.

References

Alexander, M. A., Blade, I., Newman, M., Lanzante, J. R., Lau, N.-C., and Scott, J. D.: The atmospheric bridge: the influence of ENSO teleconnections on air-sea interaction over the global oceans, J. Climate, 15, 2205–2231, 2002.

Bates, N. R.: Interannual variability of the oceanic CO_2 sink in the subtropical gyre of the North Atlantic Ocean over the last 2 decades, J. Geophys. Res., 112, C09013, doi:10.1029/2006JC003759, 2007.

Bernard, B., Madec, G., Penduff, T., Molines, J.-M., Treguier, A.-M., Sommer, J. L., Beckmann, A., Biastoch, A., Böning, C., Dengg, J., Derval, C., Durand, E., Gulev, S., Remy, E., Talandier, C., Theetten, S., Maltrud, M., McClean, J., and Cuevas, B. D.: Impact of partial steps and momentum advection schemes in a global ocean circulation model at eddy-permitting resolution, Ocean Dynam., 56, 543–567, doi:10.1007/s10236-006-0082-1, 2006.

Cooper, D. J., Watson, A. J., and Ling, R. D.: Variation of pCO_2 along a North Atlantic shipping route (UK to the Caribbean): a year of automated observations, Mar. Chem., 72, 151–169, 1998.

Chierici, M., Fransson, A., and Nojiri, Y.: Biogeochemical processes as drivers of surface fCO_2 in contrasting provinces in the subarctic North Pacific Ocean, Global Biogeochem. Cy., 20, GB1009, doi:10.1029/2004GB002356, 2006.

Dore, J. E., Lukas, R., Sadler, D. W., Church, M. J., and Karl, D. M.: Physical and biogeochemical modulation of ocean acidification in the Central North Pacific, P. Natl. Acad. Sci. USA, 106, 12235–12240, doi:10.1073/pnas.0906044106, 2009.

BGD
10, 4575–4610, 2013

Dugdale, R. C. and Wilkerson, F. P.: Low specific nitrate uptake rate: a common feature of high-nutrient, low-chlorophyll marine ecosystems, Limnol. Oceanogr., 36, 1678–1688, 1991.
Feely, R. A., Gammon, R. H., Taft, B. A., Pullen, P. E., Waterman, L. S., Conway, T. J., Gendron, J. F., and Wisegarver, D. P.: Distribution of chemical tracers in the eastern Equatorial Pacific during and After the 1982–83 El Nino/Southern Oscillation Event, J. Geophys. Res., 92, 6545–6558, 1987.
Feely, R. A., Takahashi, T., Wanninkhof, R., McPhaden, M. J., Cosca, C. E., Sutherland, S. C., and Carr, M.-E.: Decadal variability of the air-sea CO_2 fluxes in the equatorial Pacific Ocean, J. Geophys. Res., 111, C08S90, doi:10.1029/2005JC003129, 2006.
Ferry, N., Parent, L., Garric, G., Barnier, B., Jourdain, N. C., and the Mercator Ocean team: Mercator global eddy permitting ocean reanalysis GLORYS1V1: description and results, Mercator Ocean Q. Newsl., 36, 15–27, 2010.
Fransson, A., Chierici, M., and Nojiri, Y.: Increased net CO_2 outgassing in the upwelling region of the southern Bering Sea in a period of variable marine climate between 1995 and 2001, J. Geophys. Res., 111, C08008, doi:10.1029/2004JC002759, 2006.
Friedrich, T. and Oschlies, A.: Neural network-based estimates of North Atlantic surface pCO_2 from satellite data: a methodological study, J. Geophys. Res., 114, C03020, doi:10.1029/2007JC004646, 2009a.
Friedrich, T. and Oschlies, A.: Basin-scale pCO_2 maps estimated from ARGO float data: a model study, J. Geophys. Res., 114, C10012, doi:10.1029/2009JC005322, 2009b
GLOBALVIEW-CO2: Cooperative Atmospheric Data Integration Project – Carbon Dioxide, NOAA ESRL, Boulder, Colorado, available at: http://www.esrl.noaa.gov/gmd/ccgg/globalview/, 2011.
Imai, K., Nojiri, Y., Tsurushima, N., and Saino, T.: Time series of seasonal variation of primary productivity at station KNOT (44° N, 155° E) in the sub-arctic western North Pacific, Deep-Sea Res. Pt. II, 49, 5395–5408, 2002.
Inoue, H. Y., Matsueda, H., Ishii, M., Fushimi, K., Hirota, M., Asanuma, I., and Takasugi, Y.: Long-term trend of the partial pressure of carbon dioxide (pCO_2) in surface waters of the western North Pacific 1984–1993, Tellus B, 47, 391–413, 1995.
IPCC: Climate Change 2007: The Physical Science Basis. Contribution of Working Group I to the Fourth Assessment Report of the Intergovernmental Panel on Climate Change, edited by: Solomon, S., Qin, D., Manning, M., Chen, Z., Marquis, M., Averyt, K. B., Tignor, M., and Miller, H. L., Cambridge University Press, Cambridge, UK and New York, NY, USA, 2007.

BGD
10, 4575–4610, 2013

Ishii, M., Inoue, H. Y., Midorikawa, T., Saito, S., Tokieda, T., Sasano, D., Nakadate, A., Nemoto, K., Metzl, N., Wong, C. S., and Feely, R. A.: Spatial variability and decadal trend of the oceanic CO_2 in the western equatorial Pacific warm/fresh water, Deep-Sea Res. Pt. II, 56, 591–606, doi:10.1016/j.dsr2.2009.01.002, 2009.

Jamet, C., Moulin, C., and Lefèvre, N.: Estimation of the oceanic pCO_2 in the North Atlantic from VOS lines in-situ measurements: parameters needed to generate seasonally mean maps, Ann. Geophys., 25, 2247–2257, 2007, http://www.ann-geophys.net/25/2247/2007/.

Kameda, T.: Studies on oceanic primary production using ocean color remote sensing data, Bull. Fish. Res. Agen., 9, 118–148, 2003.

Karl, D. M. and Letelier, R. M.: Nitrogen fixation-enhanced carbon sequestration in low nitrate, low chlorophyll seascapes, Mar. Ecol.-Prog. Ser., 354, 257–268, doi:10.3354/meps07547, 2008.

Kohonen, T.: Self-Organizing Maps, 3rd, extended edn., Springer-Verlag, Berlin, Heidelberg, New York, 501 pp., 2001.

Kurihara, Y., Sakurai, T., and Kuragano, T.: Global daily sea surface temperature analysis using data from satellite microwave radiometer, satellite infrared radiometer and in-situ observations, Sokkou Jihou, 73, S1–S18, 2006.

Lefèvre, N., Watson, A. J., and Watson, A. R.: A comparison of multiple regression and neural network techniques for mapping in situ pCO_2 data, Tellus B, 57, 375–384, doi:10.1111/j.1600-0889.2005.00164.x, 2005.

Midorikawa, T., Ishii, M., Nemoto, K., Kamiya, H., Nakadate, A., Masuda, S., Matsueda, H., Nakano, T., and Inoue, H. Y.: Interannual variability of winter oceanic CO_2 and air-sea CO_2 flux in the western North Pacific for 2 decades, J. Geophys. Res., 111, C07S02, doi:10.1029/2005JC003095, 2006.

Murphy, P. P., Nojiri, Y., Fujinuma, Y., Wong, C. S., Zeng, J., Kimoto, T., and Kimoto, H.: Measurements of Surface Seawater fCO_2 from volunteer commercial ships: techniques and experiences from Skaugran, J. Atmos. Ocean. Tech., 18, 1719–1734, 2001a.

Murphy, P. P., Nojiri, Y., Harrison, D. E., and Larkin, N. K.: Scales of spatial variability for surface ocean pCO_2 in the Gulf of Alaska and Bering Sea: toward a sampling strategy, Geophys. Res. Lett., 28, 1047–1050, 2001b.

BGD
10, 4575–4610, 2013

Olsen, A., Bellerby, R. G. J., Johannessen, T., Omar, A., and Skjelvan, I.: Interannual variability in the wintertime air-sea flux of carbon dioxide in the northern North Atlantic, 1981–2001, Deep-Sea Res. Pt. I, 50, 1323–1338, 2003.

Patra, P. K., Maksyutov, S., Ishizawa, M., Nakazawa, T., Takahashi, T., and Ukita, J.: Interannual and decadal changes in the sea-air CO_2 flux from atmospheric CO_2 inverse modeling, Global Biogeochem. Cy., 19, GB4013, doi:10.1029/2004GB002257, 2005.

Pfeil, B., Olsen, A., Bakker, D. C. E., Hankin, S., Koyuk, H., Kozyr, A., Malczyk, J., Manke, A., Metzl, N., Sabine, C. L., Akl, J., Alin, S. R., Bellerby, R. G. J., Borges, A., Boutin, J., Brown, P. J., Cai, W.-J., Chavez, F. P., Chen, A., Cosca, C., Fassbender, A. J., Feely, R. A., González-Dávila, M., Goyet, C., Hardman-Mountford, N., Heinze, C., Hood, M., Hoppema, M., Hunt, C. W., Hydes, D., Ishii, M., Johannessen, T., Jones, S. D., Key, R. M., Körtzinger, A., Landschützer, P., Lauvset, S. K., Lefèvre, N., Lenton, A., Lourantou, A., Merlivat, L., Midorikawa, T., Mintrop, L., Miyazaki, C., Murata, A., Nakadate, A., Nakano, Y., Nakaoka, S., Nojiri, Y., Omar, A. M., Padin, X. A., Park, G.-H., Paterson, K., Perez, F. F., Pierrot, D., Poisson, A., Ríos, A. F., Santana-Casiano, J. M., Salisbury, J., Sarma, V. V. S. S., Schlitzer, R., Schneider, B., Schuster, U., Sieger, R., Skjelvan, I., Steinhoff, T., Suzuki, T., Takahashi, T., Tedesco, K., Telszewski, M., Thomas, H., Tilbrook, B., Tjiputra, J., Vandemark, D., Veness, T., Wanninkhof, R., Watson, A. J., Weiss, R., Wong, C. S., and Yoshikawa-Inoue, H.: A uniform, quality controlled Surface Ocean CO_2 Atlas (SOCAT), Earth Syst. Sci. Data Discuss., 5, 735–780, doi:10.5194/essdd-5-735-2012, 2012.

Sabine, C. L., Feely, R. A., Gruber, N., Key, R. M., Lee, K., Bullister, J. L., Wanninkhof, R., Wong, C. S., Wallace, D. W. R., Tilbrook, B., Millero, F. J., Peng, T.-H., Kozyr, A., Ono, T., and Rios, A. F.: The oceanic sink for anthropogenic CO_2, Science, 305, 367, doi:10.1126/science.1097403, 2004.

Sabine, C., Maenner, S., and Sutton, A.: High-resolution ocean and atmosphere pCO_2 time-series measurements from mooring Papa_145W_50N, Carbon Dioxide Information Analysis Center, Oak Ridge National Laboratory, US Department of Energy, Oak Ridge, Tennessee, doi:10.3334/CDIAC/otg.TSM_Papa_145W_50N, 2010.

Sabine, C. L., Hankin, S., Koyuk, H., Bakker, D. C. E., Pfeil, B., Olsen, A., Metzl, N., Kozyr, A., Fassbender, A., Manke, A., Malczyk, J., Akl, J., Alin, S. R., Bellerby, R. G. J., Borges, A., Boutin, J., Brown, P. J., Cai, W.-J., Chavez, F. P., Chen, A., Cosca, C., Feely, R. A., González-Dávila, M., Goyet, C., Hardman-Mountford, N., Heinze, C., Hoppema, M., Hunt, C. W., Hydes, D., Ishii, M., Johannessen, T., Key, R. M., Körtzinger, A., Landschützer, P., Lau-

BGD
10, 4575–4610, 2013

vset, S. K., Lefèvre, N., Lenton, A., Lourantou, A., Merlivat, L., Midorikawa, T., Mintrop, L., Miyazaki, C., Murata, A., Nakadate, A., Nakano, Y., Nakaoka, S., Nojiri, Y., Omar, A. M., Padin, X. A., Park, G.-H., Paterson, K., Perez, F. F., Pierrot, D., Poisson, A., Ríos, A. F., Salisbury, J., Santana-Casiano, J. M., Sarma, V. V. S. S., Schlitzer, R., Schneider, B., Schuster, U., Sieger, R., Skjelvan, I., Steinhoff, T., Suzuki, T., Takahashi, T., Tedesco, K., Telszewski, M., Thomas, H., Tilbrook, B., Vandemark, D., Veness, T., Watson, A. J., Weiss, R., Wong, C. S., and Yoshikawa-Inoue, H.: Surface Ocean CO_2 Atlas (SOCAT) gridded data products, Earth Syst. Sci. Data Discuss., 5, 781–804, doi:10.5194/essdd-5-781-2012, 2012.

Sarma, V. V. S. S., Saino, T., Sasaoka, K., Nojiri, Y., Ono, T., Ishii, M., Inoue, H. Y., and Matsumoto, K.: Basin-scale pCO_2 distribution using satellite sea surface temperature, Chl *a*, and climatological salinity in the North Pacific in spring and summer, Global Biogeochem. Cy., 20, GB3005, doi:10.1029/2005GB002594, 2006.

Schmitz Jr., W. J. (Ed.): On the World Ocean Circulation: Volume I; Some Global Features/North Atlantic Circulation, Tech. Rept., Woods Hole Oceanogr. Inst., Woods Hole, Massachusetts 02543, 1996.

Schuster, U., Watson, A. J., Bates, N. R., Corbiére, A., González-Dávila, M., Metzl, N., Pierrot, D., and Santana-Casiano, M.: Trends in North Atlantic sea-surface fCO_2 from 1990 to 2006, Deep-Sea Res. Pt. II, 56, 620–629, 2009.

Takahashi, T., Olafsson, J., Godard, J. G., Chipman, D. W., and Sutherland, S. C.: Seasonal variation of CO_2 and nutrient in the high-latitude surface oceans: a comparative study, Global Biogeochem. Cy., 7, 843–878, 1993.

Takahashi, T., Sutherland, S. C., Feely, R. A., and Wanninkhof, R.: Decadal change of the surface water pCO_2 in the North Pacific: a synthesis of 35 years of observations, J. Geophys. Res., 111, C07S05, doi:10.1029/2005JC003074, 2006.

Takahashi, T., Sutherland, S. C., Wanninkhof, R., Sweeney, C., Feely, R. A., Chipman, D. W., Hales, B., Friederich, G., Chavez, F., Watson, A., Bakker, D. C. E., Schuster, U., Metzl, N., Inoue, H. Y., Ishii, M., Midorikawa, T., Sabine, C. L., Hopemma, M., Olafsson, J., Arnarson, T. S., Tilbrook, B., Johannessen, T., Olsen, A., Bellerby, R., de Baar, H. J. W., Nojiri, Y., Wong, C. S., and Delille, B.: Climatological mean and decadal change in surface ocean pCO_2, and net sea-air CO_2 flux over the global oceans, Deep-Sea Res. Pt. II, 56, 554–577, doi:10.1016/j.dsr2.2008.12.009, 2009.

Takamura, T. R., Inoue, H. Y., Midorikawa, T., Ishii, M., and Nojiri, Y.: Seasonal and inter-annual variations in pCO_2^{sea} and air-sea CO_2 fluxes in mid-latitudes of the western and eastern North

BGD
10, 4575–4610, 2013

Pacific during 1999–2006: recent results utilizing voluntary observation ships, J. Meteorol. Soc. Jpn., 88, 883–898, doi:10.2151/jmsj.2010-602, 2010.

Telszewski, M., Chazottes, A., Schuster, U., Watson, A. J., Moulin, C., Bakker, D. C. E., González-Dávila, M., Johannessen, T., Körtzinger, A., Lüger, H., Olsen, A., Omar, A., Padin, X. A., Ríos, A. F., Steinhoff, T., Santana-Casiano, M., Wallace, D. W. R., and Wanninkhof, R.: Estimating the monthly pCO_2 distribution in the North Atlantic using a self-organizing neural network, Biogeosciences, 6, 1405–1421, doi:10.5194/bg-6-1405-2009, 2009.

Trenberth, K. E. and Caron, J. M.: The Southern Oscillation revisited: sea level pressures, surface temperatures and precipitation, J. Climate, 13, 4358–4365, 2000.

Usui, N., Ishizaki, S., Fujii, Y., Tsujino, H., Yasuda, T., and Kamachi, M.: Meteorological Research Institute multivariate ocean variational estimation (MOVE) system: some early results, Adv. Space Res., 37, 806–822, doi:10.1016/j.asr.2005.09.022, 2006.

Valsala, V., Maksyutov, S., Telszewski, M., Nakaoka, S., Nojiri, Y., Ikeda, M., and Murtugudde, R.: Climate impacts on the structures of the North Pacific air-sea CO_2 flux variability, Biogeosciences, 9, 477–492, doi:10.5194/bg-9-477-2012, 2012.

Wakita, M., Watanabe, S., Murata, A., Tsurushima, N., and Honda, M.: Decadal change of dissolved inorganic carbon in the subarctic western North Pacific Ocean, Tellus B, 62, 608–620, doi:10.1111/j.1600-0889.2010.00476.x, 2010.

Wong, C. S., Christian, J. R., Emmy Wong, S.-K., Page, J., Xie, L., and Johannessen, S.: Carbon dioxide in surface seawater of the eastern North Pacific Ocean (Line P), 1973–2005, Deep-Sea Res. Pt. I, 57, 687–695, doi:10.1016/j.dsr.2010.02.003, 2010.

Wong, C. S. and Johannessen, S.: Sea Surface and Atmospheric pCO_2 Data in the Pacific Ocean During the Station P Cruises from 1973–2003, Carbon Dioxide Information Analysis Center, Oak Ridge National Laboratory, US Department of Energy, Oak Ridge, Tennessee, doi:10.3334/CDIAC/otg.VOS_station_p_ca, 2010.

Zeng, J., Nojiri, Y., Murphy, P. P., Wong, C. S., and Fujinuma, Y.: A comparison of ΔpCO_2 distributions in the northern North Pacific using results from a commercial vessel in 1995–1999, Deep-Sea Res. Pt. II, 49, 5303–5315, 2002.

BGD
10, 4575–4610, 2013

Table 1. Summary of NIES surface ocean CO_2 measurements made by four volunteer observing ships in the Pacific Ocean.

Vessel name	Period	Observed area	NDIR analyzer
M/S *Skaugran*	Mar 1995–Sep 1999	North Pacific	Rosemount Analytical Model 880A
M/S *Alligator Hope*	Nov 1999–Mar 2001	North Pacific	Licor 6262
M/S *Pyxis*	Jul 2002–present	North Pacific	Licor 6262 (–Apr 2006) Licor 7000 (Apr 2006–)
M/S *Trans Future 5*	Jul 2006–present	Western North/ South Pacific	Licor 6262

BGD
10, 4575–4610, 2013

Table 2. Ranges of SST, MLD, CHL and SSS in the training dataset, the labeling dataset and the trained neurons. Percentages of the training data within the range of the labeling dataset and the neurons are given for each parameter.

	SST (°C)			MLD (m)			CHL ($mg\,m^3$)			SSS (psu)		
	Min	Max	cover (%)	Min	Max	cover (%)	Min	Max	cover (%)	Min	Max	cover (%)
Training data	−1.8	32.7		1	> 500		0.00	10		30.15	35.69	
Labeling data	−1.1	31.5	99.940	1	416	99.995	0.00	10	100	30.15	35.69	100
Neurons	−0.6	29.4	96.651	1	194	99.807	0.00	3.2	99.778	31.79	35.58	99.886

BGD
10, 4575–4610, 2013

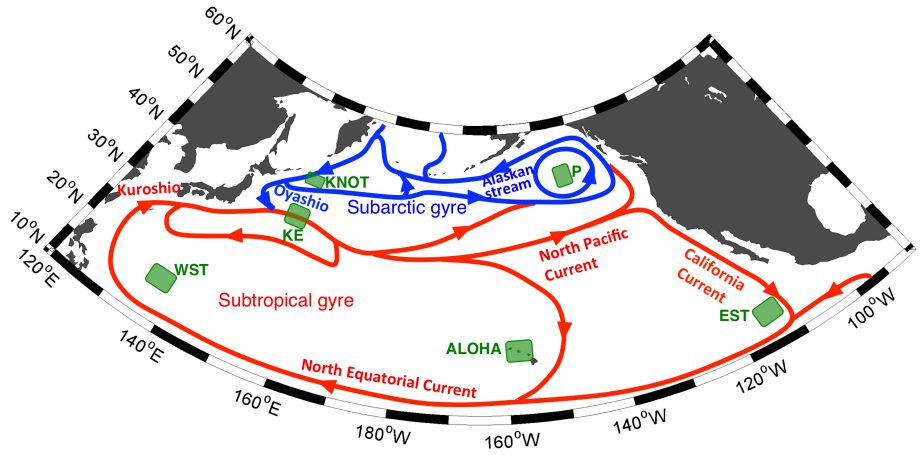

Fig. 1. Schematic map of the current system in the North Pacific rewritten from Schmitz (1996) with the areas of three ocean time-series stations and three areas for comparison of seasonal and interannual variations of pCO_2^{sea} and related oceanic parameters "KNOT", "P", and "ALOHA" denote ocean time-series station areas in the North Pacific, and "WST", "KE", and "EST" denote ocean areas of the western subtropics, Kuroshio extension, and eastern subtropics, respectively.

BGD
10, 4575–4610, 2013

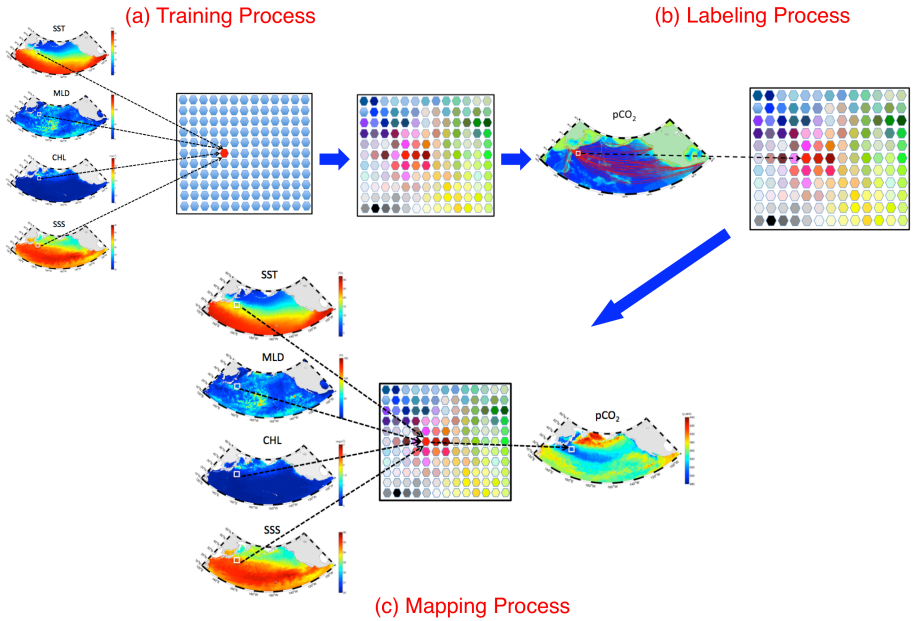

Fig. 2. Visualization of the processes that make up the procedure for SOM analysis.

BGD
10, 4575–4610, 2013

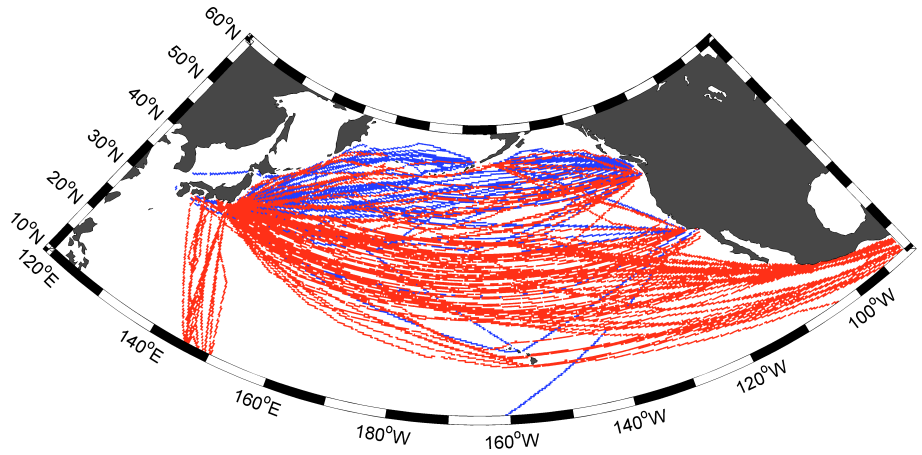

Fig. 3. Composite cruise tracks from 1998 to 2008. Blue lines represent the cruises from 1998 to 2001 and red lines show the cruises after 2002.

BGD
10, 4575–4610, 2013

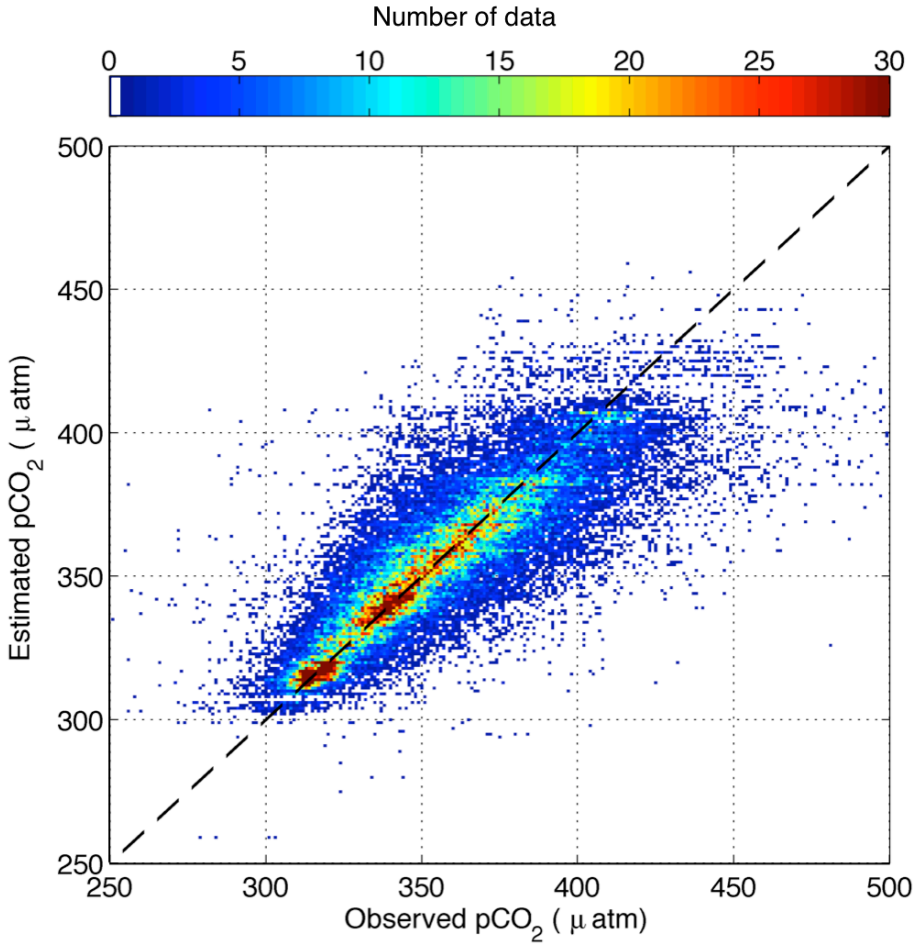

Fig. 4. Scatter plot of estimated pCO_2^{sea} with observed pCO_2^{sea}. Colors indicate the number of data in a 1 µatm × 1 µatm bin.

BGD
10, 4575–4610, 2013

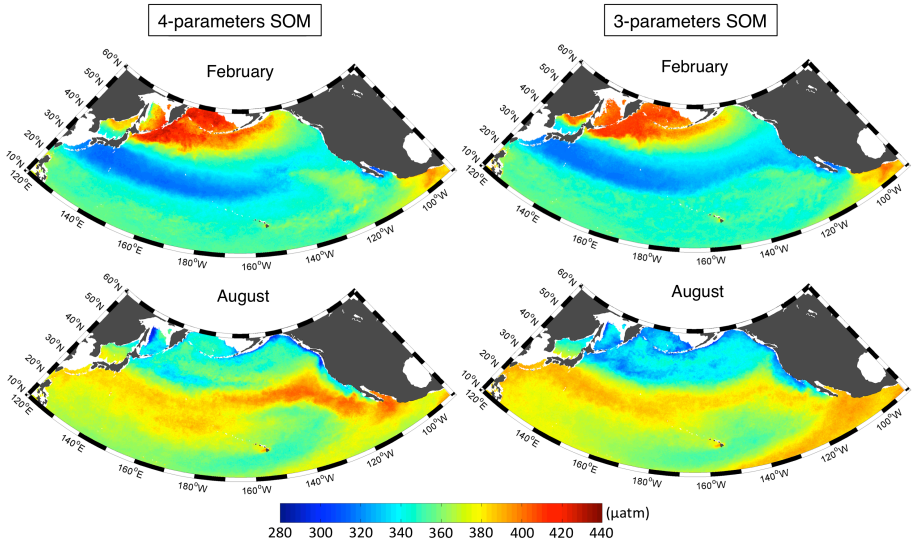

Fig. 5. Comparison of seven-year averaged monthly pCO_2^{sea} distributions from 2002 to 2008 in February (upper) and August (bottom). Figures on the left are the pCO_2^{sea} distributions estimated from the four-parameter SOM including SSS. Figures on the right were estimated from the three-parameter SOM without SSS.

BGD
10, 4575–4610, 2013

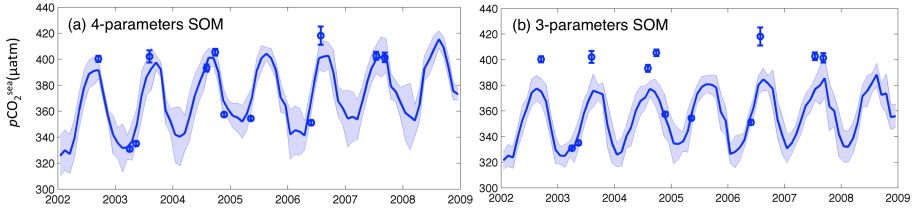

Fig. 6. The pCO_2^{sea} variations in the area (36° N to 38° N, 138° W to 142° W) where the North Pacific current flows, estimated by the four-parameter SOM including SSS **(a)** and the three-parameter SOM without SSS **(b)**. The blue lines and the shaded areas indicate the mean values of the estimated pCO_2^{sea} and the spatial variability (2-σ) calculated in the area, respectively. Blue circles are the in situ pCO_2^{sea} values obtained from the NIES VOS program. The pCO_2^{sea} observations in the target areas include several grid points binned by 0.25° latitude × 0.25° longitude resolution, and the bar indicates the spatial variability (1-σ).

BGD
10, 4575–4610, 2013

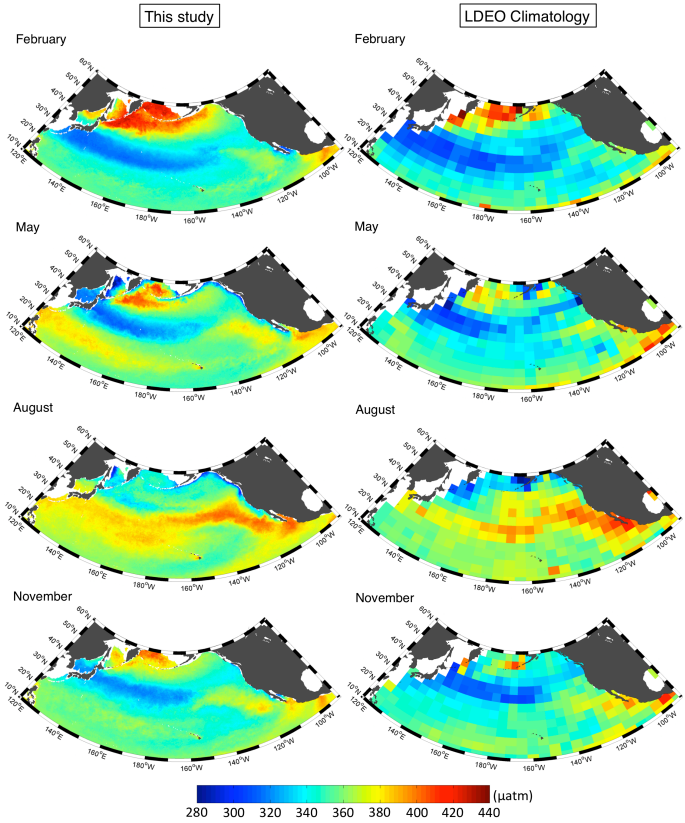

Fig. 7. Distributions of the seven-year averaged monthly mean pCO_2^{sea} in this study (panels on left) and the LDEO monthly pCO_2^{sea} climatology (panels on right, but with 8.8 µatm added to the maps to change the reference year from 2000 to 2005) for February, May, August, and November.

BGD
10, 4575–4610, 2013

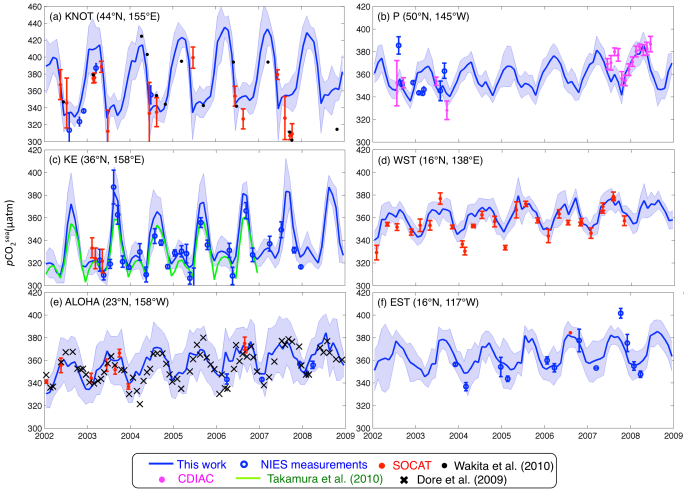

Fig. 8. Interannual variation of pCO_2^{sea} (μ atm) within time-series station areas and within ocean areas. The blue solid lines and shaded areas show the monthly pCO_2^{sea} values and the spatial variability (2-σ) calculated in the respective areas. The grid size of all the averaged areas except in the Station KNOT area is set to 4° latitude × 5° longitude, whereas the Station KNOT area is set to 43.5° N to 45.5° N, 153° E to 157° E. Blue circles and red dots are in situ pCO_2^{sea}/fCO_2^{sea} values obtained from NIES measurements and the SOCAT database, respectively. Black dots and crosses on panel **(a)** and **(c)** are the pCO_2^{sea} values calculated from measurements of DIC and TA reported by Wakita et al. (2010) and Dore et al. (2009). Purple dots on panel **(b)** are the pCO_2^{sea} values observed by Wong and Johansen (2010) and Sabine et al. (2010). In panel **(c)**, the solid green line denotes the pCO_2^{sea} values during the 2002–2006 period estimated by Takamura et al. (2010). Note that the range of the ordinate in the Station KNOT area is larger than those of other station areas.

BGD
10, 4575–4610, 2013

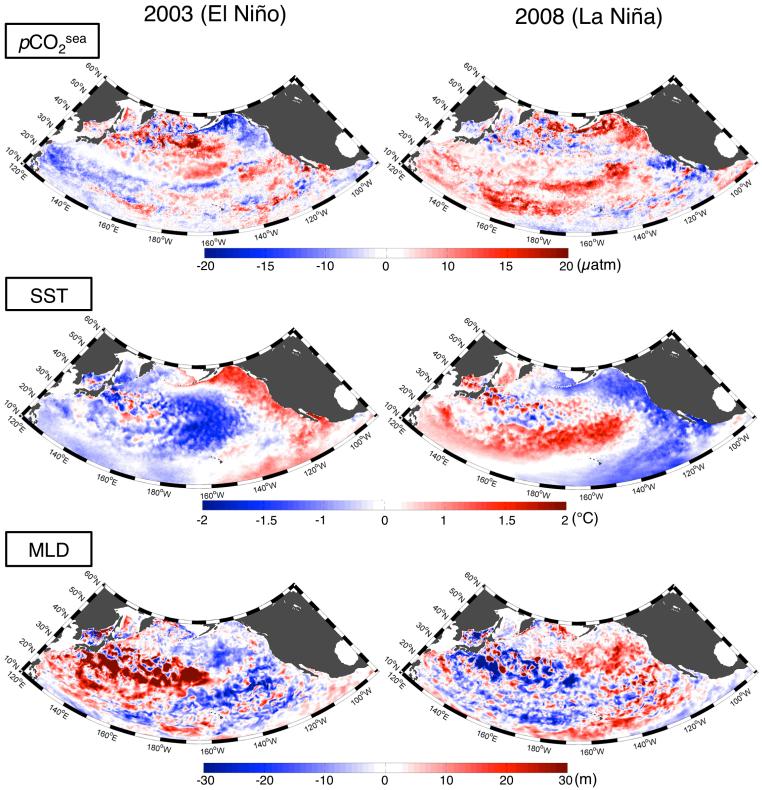

Fig. 9. Anomalies from the monthly climatology for the period 2002–2008 for de-trending pCO_2^{sea} (upper), SST (middle), and MLD (bottom) distributions during the winter of 2003 (panels on left) and 2008 (panels on right).

BGD
10, 4575–4610, 2013